Why does vacuum drive to the loading of halloysite nanotubes? The key role of water confinement

Lorenzo Lisuzzo[a], Giuseppe Cavallaro[a,b*], Pooria Pasbakhsh[c], Stefana Milioto[a,b], Giuseppe Lazzara[a,b]

[a]*Dipartimento di Fisica e Chimica, Università degli Studi di Palermo, Viale delle Scienze, pad. 17, 90128 Palermo, Italy.*

[b]*Consorzio Interuniversitario Nazionale per la Scienza e Tecnologia dei Materiali, INSTM, Via G. Giusti, 9, I-50121 Firenze, Italy*

[c]*Mechanical Engineering Discipline, School of Engineering, Monash University Malaysia, 47500 Selangor, Malaysia*

Abstract

The filling of halloysite nanotubes with active compounds solubilized in aqueous solvent was investigated theoretically and experimentally. Based on Knudsen thermogravimetric data, we demonstrated the water confinement within the cavity of halloysite. This process is crucial to properly describe the driving mechanism of halloysite loading. In addition, Knudsen thermogravimetric experiments were conducted on kaolinite nanoplates as well as on halloysite nanotubes modified with an anionic surfactant (sodium dodecanoate) in order to explore the influence of both the nanoparticle morphology and the hydrophobic/hydrophilic character of the lumen on the confinement phenomenon. The analysis of the desorption isotherms allowed us to determine the water adsorption properties of the investigated nanoclays. The pore sizes of the nanotubes' lumen was determined by combining the vapor pressure of the confined water with the nanoparticles wettability, which was studied through contact angle measurements. The thermodynamic description of the water confinement inside the lumen was correlated to the influence of the vacuum pumping in the experimental loading of halloysite. Metoprolol tartrate, salicylic acid and malonic acid were selected as anionic guest molecules for the experimental filling of the positively charged halloysite lumen. According to the filling mechanism induced by the water confinement, the vacuum operation and the reduced pressure enhanced the loading of halloysite nanotubes for all the investigated bioactive compounds.

This work represents a further and crucial step for the development of halloysite based nanocarriers being that the filling mechanism of the nanotube's cavity from aqueous dispersions was described according to the water confinement process.

Keywords: halloysite, nanotubes, water confinement, clay nanoparticles, loading mechanism, vacuum pumping.

1. Introduction

The encapsulation of active molecules within the cavity of tubular nanoparticles represents an emerging issue because of its implications on the fundamental sciences and nanotechnologies.[1–7] Literature[2] reports that the filling of carbon nanotubes from aqueous solutions depends on the confinement of water, which exhibits an increase of its boiling temperature. Kim at al.[1] evidenced that the loading of carbon nanotubes is driven by the peculiar evaporation process occurring in the confined space.

Among the nanoparticles with tubular morphology, halloysite nanoclay has attracted a growing interest because of its biocompatibility, geometrical characteristics and peculiar surface properties.[8,9] Due to its high specific surface, halloysite was employed as efficient catalytic support for the deposition of Pd[10,11] and Ag nanoparticles and bimetallic catalysts, such as Cu-Co[12] and AgPd.[13] As concerns the biocompatibility, halloysite nanotubes (HNTs) revealed a low toxicity towards nematodes,[14] mice[15] and microorganisms.[16,17] In vitro tests showed that halloysite generates a very low cytotoxicity on human cells, such as endothelial[18] and epithelial[19] cells as well as peripheral blood lymphocytes[20]

As described in a recent review,[3] halloysite possess a hollow tubular structure as a consequence of the rolling of kaolinite nanosheets. According to both microscopy[21] and scattering results,[22] the geological origin affects the sizes and the corresponding polydispersion degree of halloysite nanotubes. The HNTs length is about 1 μm, while the external and inner diameters are within 20−200 and 10−70 nm, respectively. Halloysite belongs to the mineralogical class of 1:1 phyllosilicates being that the component layers are formed by two sheets with different configuration (one octahedral sheet of alumina and one tetrahedral sheet of silica). As a consequence of the rolling of the sheets,[23] the inner and outer surfaces of halloysite possess different chemical composition and opposite charge within a pH range between 2 and 8. Specifically, the alumina internal surface is positively charged, while the silica shell presents a negative charge.[24] Consequently, electrostatic attractive forces between ionic molecules and the

charged halloysite surfaces drives to the selective functionalization of the clay nanotubes.[25] As example, the adsorption of sodium alkanoates onto the HNTs inner surfaces generated inorganic tubular micelles with excellent removal ability towards hydrocarbons (both aliphatic and aromatic)[26] as well as organic dyes.[25] It was demonstrated that the peculiar interfaces of halloysite control the self-assembling processes,[27,28] the formation of liquid crystals[29] and the preparation of Pickering emulsions,[30,31] which can be used for oil spill remediation.

Several studies[32–38] showed that HNTs can be employed as nanocontainers for biologically and chemically active compounds, which are filled within the confined space of the halloysite lumen. The sustained release of the entrapped molecules extends their action time, which can be exploited for specific pharmaceutical, medical and technological purposes.[35] The combination of ecocompatible polymers and loaded HNTs generated composite films with antioxidant[39,40] anticorrosive[34,41] and antimicrobial activities[3,42,43] that are useful for food packaging, protection coatings and tissue engineering.

The most common procedure for the HNTs loading consists of three steps: 1) mixing of the clay dry powder with the saturated solution of the guest molecule; 2) sonication and stirring of the HNTs/guest molecule dispersion; 3) vacuum pumping in/out operation, in which the dispersion is transferred from atmospheric pressure to a vacuum jar. The latter step was introduced with the aim to optimize the amount of active molecules loaded inside the nanotubes by keeping the system under vacuum for 1-5 h and then cycling it back to atmospheric pressure. Generally, this operation is repeated for 3 times. The first demonstration on the usage of vacuum pumping for an enhancement of the drug loading inside the HNTs cavity is reported by Price et al.[44] The influence of the vacuum pumping on the filling mechanism of HNTs lumen is still unclear. Macroscopically, we observe a slight fizzing of the HNTs suspension under vacuum. Firstly, this observation was related to the air removal from the HNTs inner space and the consequent promotion of the filling of the drug solution.[45–47] The most recent hypothesis report that the vacuum conditions increase the

loading efficiency because of the water removal from the nanotubes occurring during the observed slight fizzing.[35]

Here, we explored the loading mechanism by focusing on the unusual thermodynamics of water restrained inside a confined space. According to the Gibbs-Thomson effect,[48] the curvature of the HNTs cavity increases the water vapor pressure and, consequently, the evaporation process is faster. Namely, the increase of the vapor pressure is related to the surface/volume ratio, which is enhanced for water confined within the HNTs pores. In general, the dependence of the vapor pressure P(r) of a liquid on the curvature of the pores is expressed by the Kelvin equation

$$P(r) = P^{\infty} \exp(\gamma/r \cdot \rho \cdot k_B \cdot T) \quad (1)$$

where P^{∞} is the vapour pressure of the bulk liquid, γ is the surface tension, r is the pore radius, ρ is the density, k_B is the Boltzmann constant and T is the temperature.

In our previous study,[48] the filling of n-decane within the hydrophobically modified HNTs was proved by the significant decrease (ca. 40 °C) of the volatilization temperature for the confined hydrocarbon. This finding highlights the relevant effect of the confinement phenomenon on the liquid volatilization and, consequently, on its tendency to move from the HNTs cavity.

Based on these considerations, this work was aimed to 1) demonstrate the water confinement inside the HNTs cavity; 2) provide a clear and unequivocal description of the HNTs filling from aqueous solutions of guest molecules. Accordingly, the attained knowledge could open new routes in the preparation procedure of effective delivery systems based on clay nanotubes.

2. Experimental

2.1. Materials

Halloysite nanotubes (HNTs), kaolinite (Kao), sodium dodecanoate (NaL) and metoprolol tartrate (MT) are Sigma Aldrich products. Salicylic acid (SA) and malonic acid (MA) are from Fluka and Acros Organics, respectively. All the products were used without any purification treatment.

2.2. Hydrophobization of halloysite cavity

Halloysite nanotubes with a hydrophobic cavity were prepared by using the same procedure reported in our previous papers.[25,26] Firstly, we prepared a stable NaL aqueous solution (concentration of 1.25 wt%) by magnetically stirring for 2 hours at 20 °C. Then, we added an appropriate amount of halloysite and the obtained dispersion was magnetically stirred for 48 hours at 20 °C. Based on the geometrical characteristics of halloysite, the maximum surfactant loading in the cavity is ca. 10% vol. Therefore, the selected HNT/surfactant ratio (1:1) of the suspension assures the full loading of the halloysite cavity. Afterwards, the dispersion was centrifuged allowing to recover the HNTs/NaL solid material, which was washed three times with water in order to avoid the presence of unbound surfactant. As shown by FESEM images (Figure 1), the hydrophobization of the HNTs cavity did not alter the hollow tubular shape of halloysite. For comparison, the platy morphology of kaolinite is displayed in FESEM microscopies (Figure 1).

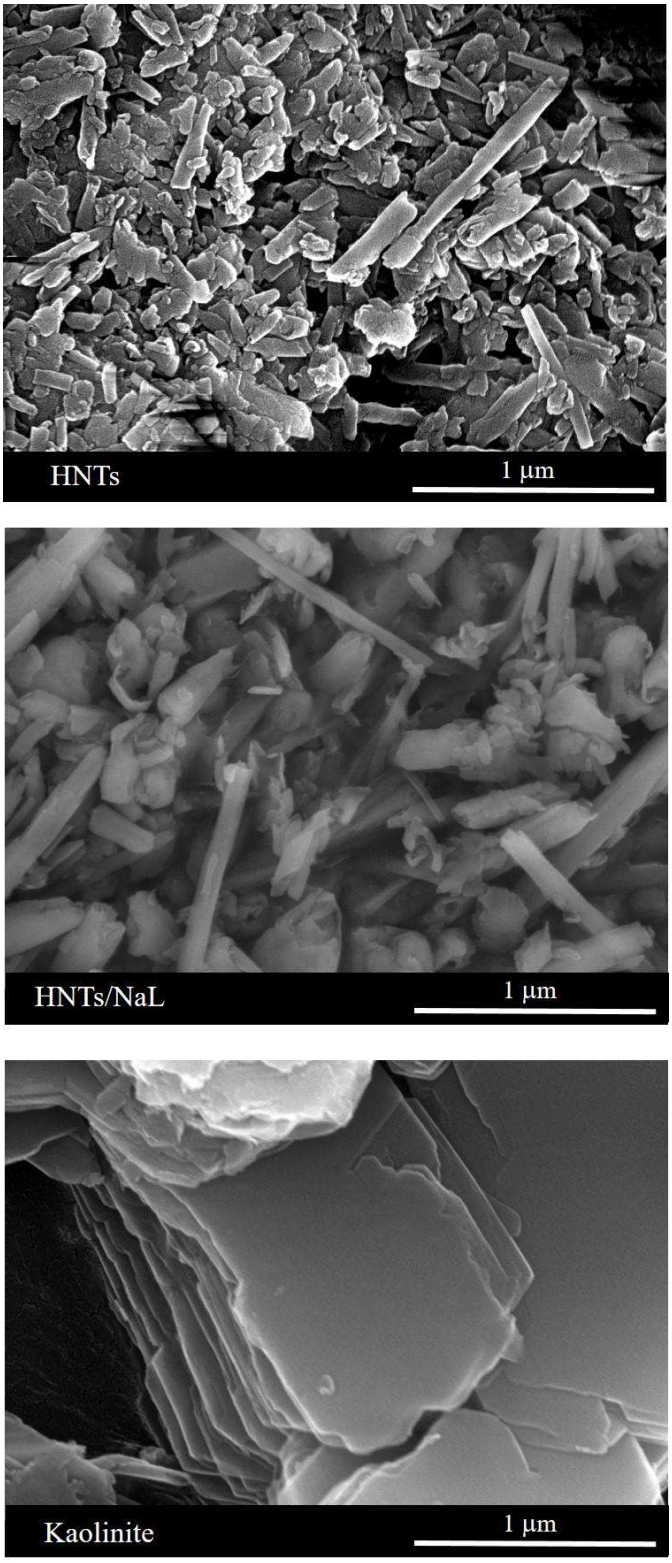

Figure 1. FESEM images for HNTs, HNTs/NaL and kaolinite

2.3. Encapsulation of active molecules within halloysite lumen

The encapsulation of the active molecules (metoprolol tartrate, salicylic acid and malonic acid) within the halloysite cavity was performed by aqueous suspensions as described elsewhere.[35] Due to their carboxylate groups, the selected guest molecules can be entrapped within the lumen as a consequence of electrostatic interactions with HNTs inner surface, which is positively charged. Firstly, we prepared saturated solutions of the active compounds in water by magnetically stirring for 2 hours at 20 °C. To these solutions, we added a certain amount of halloysite in order to obtain aqueous dispersions with a HNTs/guest molecule ratio of 2:1. The HNTs/drug suspensions were subjected to ultrasonication for 5 minutes and transferred to a vacuum jar, which allows to reduce the pressure conditions (P = 0.01 atm). The suspensions were kept under reduced pressure for 30 minutes and, then, the vacuum was broken. The cyclic vacuum pumping in/out procedure was repeated three times. Finally, the dispersions were centrifuged to recover the loaded nanotubes, which were washed three times with water to remove the unbound guest molecules. The obtained nanomaterials were dried and stored in a desiccator at room temperature. Besides the described preparation procedure, the loading of the nanotubes was carried out by keeping the HNTs/guest molecule suspensions at P = 1 atm for 90 minutes. The latter replaced the vacuum pumping in/out cycles. The comparison of the loadings at different pressure (P = 0.01 and 1 atm) allowed us to investigate the influence of the vacuum conditions on the filling process. Moreover, we conducted the loading of salicylic acid into kaolinite plates by using the same protocols employed for halloysite.

2.4 Methods

2.4.1. Thermogravimetry

Thermogravimetry (TG) measurements were performed by means of a Q5000 IR apparatus (TA Instruments) under the nitrogen flows of 25 cm^3 min^{-1} and 10 cm^3 min^{-1} for the sample and the

balance, respectively. The temperature calibration of the apparatus was conducted on the basis of the Curie temperatures of standards (nickel, cobalt, and their alloys) as reported elsewhere.[49] TG experiments were conducted on HNTs/active molecules and their pure components by heating the samples (ca. 5 mg) from room temperature to 800 °C with a scanning rate of 20 °C min^{-1}. The quantitative analysis of TG data provided the loading through the rule of mixtures.[33] Details on the calculation of the loading amounts of guest molecules are presented in Supporting Information. Moreover, Knudsen thermogravimetry (KTG) tests were conducted in isothermal conditions (temperature was fixed at 30 °C) by replacing the standard open pan with the Knudsen cell, which possesses an orifice with a diameter of 20 μm. In this regards, it should be noted that KTG analysis is a proper method to investigate the interactions between water and nanoclays, as reported for smectite.[50] KTG measurements were conducted on 30 wt% aqueous dispersions of clay samples (kaolinite, HNTs and HNTs/NaL). As shown in Supporting Information, the masses of the highly concentrated suspensions (that corresponds to wet clays) decrease with the time until a constant value, which represents the mass of the dried nanomaterials indicating that the evaporation is complete.

KTG measurements allowed us to study the isothermal water evaporation from wet nanoclays. The mass loss rate (that corresponds to the evaporation velocity) can be expressed as

$$dm/dt = K\cdot(P_{int} - P_{ext}) \quad (1)$$

where K is a constant related to the volatile gas, P_{int} is the partial pressure of the water vapor inside the cell and P_{ext} is the external pressure. Due to the small orifice of the Knudsen cell, P_{int} is much larger (at least two order) than P_{ext} and, consequently, the evaporation velocity can be considered proportional to P_{int}. On this basis, we can estimate the evolution of the thermodynamic water activity (a_w) during the evaporation according to the following equation

$$(dm/dt)_n/(dm/dt)_w \approx (P_{int})_n/(P_{int})_w = a_w \quad (2)$$

being $(dm/dt)_n$ and $(dm/dt)_w$ the mass loss rates for the nanoclay aqueous dispersion and pure water, respectively. It should be noted that $(P_{int})_w$ represents the relative vapor pressure for pure water, while $(P_{int})_n$ is the vapor pressure of water contained in the nanoclay dispersion.

Based on the KTG data analysis, we investigated the effect of the nanoparticles morphology on the relative vapor pressure of water evaporated from wet nanoclays.

2.4.2 Water contact Angle

Water contact angle tests were conducted on HNTs, HNTs/NaL and kaolinite by using an optical contact angle apparatus (OCA 20, Data Physics Instruments) equipped with a video measuring system having a high-resolution CCD camera and a high-performance digitizing adapter. Data acquisition was conducted by SCA 20 software (Data Physics Instruments). The contact angle (θ) of water in air was detected through the sessile drop method by placing a water droplet of 10 ± 0.5 mL onto the surface of nanoclay tablets. The measurements were conducted at 30.0 ± 0.1 °C. Images were collected 50 times per second, starting from the deposition of the drop to 6 s. The evolution of the water contact angle on time was fitted by an empiric approach based on the following equation[51]

$$\theta = \theta_i \cdot \exp(-k_\theta \cdot t^n) \quad (3)$$

where θ_i corresponds to the initial contact angle, k_θ and n are characteristic coefficients related to the kinetics and the mechanism of the process. Specifically, n ranges between 0 and 1 on dependence of the absorption and spreading contributions to the kinetic θ evolution.

2.4.3 Field Emission Scanning Electron Microscopy (FESEM)

FESEM experiments were carried out by means of FE-SEM, Hitachi SU8010 microsope. To prevent electrostatic charging during observation, the samples were coated with a thin layer of platinum.

3. Results and discussion

3.1 Thermodynamics of water evaporation from nanoclay aqueous dispersions: Knudesen thermogravimetry

The thermodynamics of water evaporation from halloysite nanotubes and platy-like kaolinite was explored by KTG experiments in order to investigate the effect of the nanoclay morphology on the vapor pressure of the evaporating water. Based on the KTG data analysis, we determined the dependence of the water evaporation rate on the moisture content (M_w) of the nanoclays for HNTs, HNTs/NaL and kaolinite dispersions (Figure 2). It should be noted that M_w was calculated from the mass ratio between water and dry nanoclay. The trends in Figure 2 allows to classify the evaporating water in three categories: 1) bulk water ($(dm/dt)_n/(dm/dt)_w = 1$); 2) confined water ($(dm/dt)_n/(dm/dt)_w > 1$); 3) adsorbed water ($(dm/dt)_n/(dm/dt)_w < 1$). It should be noted that halloysite possesses two interlayer water molecules per formula unit. The evaporation of the interlayer water cannot be detected by KTG experiments being that their expulsion from halloysite structure occurs at ca. 500 °C.[23]

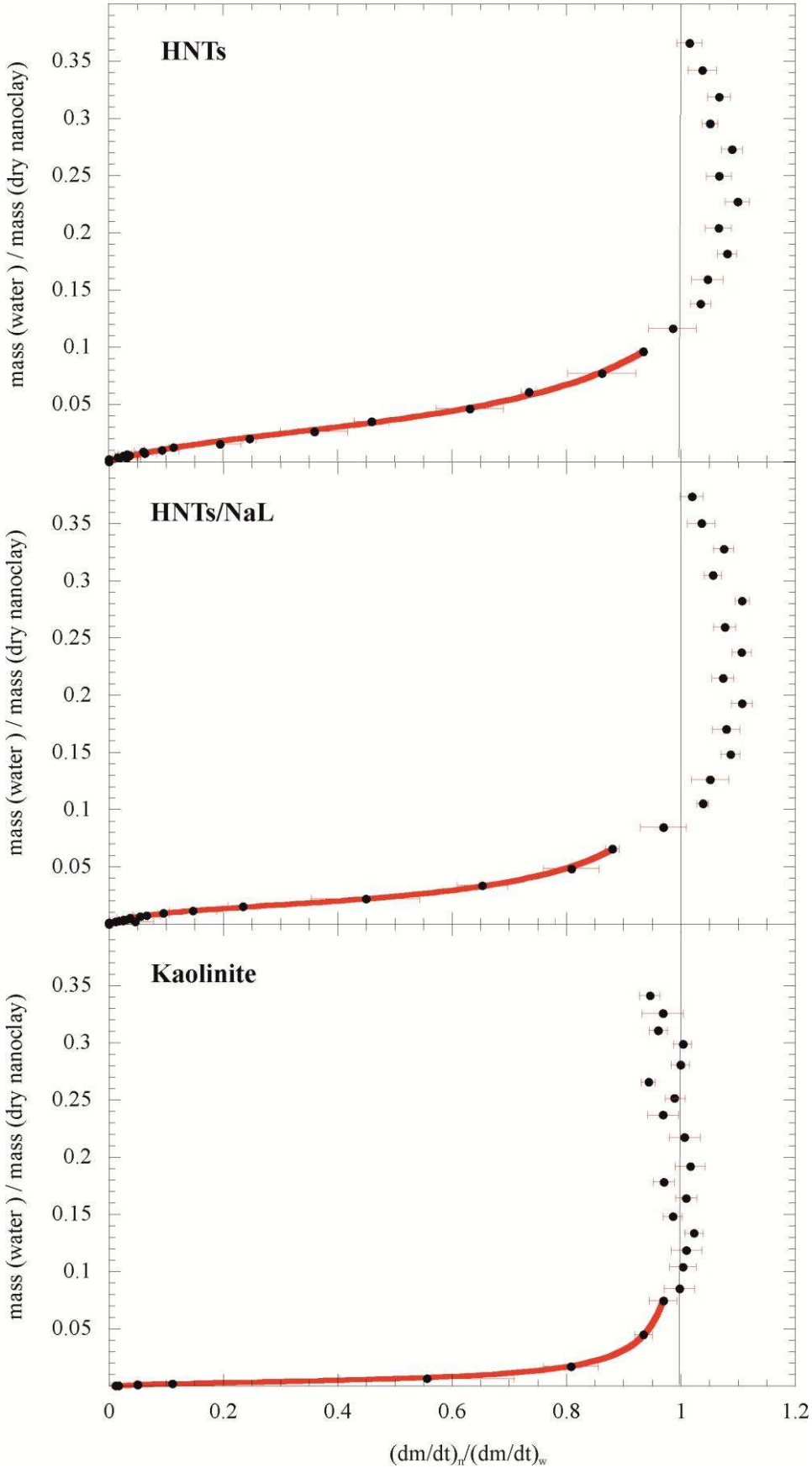

Figure 2. Mass loss rates for the nanoclay aqueous dispersions normalized for pure water evaporation as a function of the mass ratio between water and dry nanoclay. The experimental data in water activity range between 0.05 and 0.95 were fitted according to GAB model (red solid line).

3.1.1 Water confinement within the halloysite nanotubes cavity

As concerns both pure and surfactant modified halloysite (Figure 2), a large content (ca. 25 wt%) of evaporating water presents $(dm/dt)_n/(dm/dt)_w > 1$, which means that its vapor pressure is greater than that of bulk water. This result can be attributed to the confinement of water within the nanotube's cavity in agreement with the Gibbs-Thomson effect.[52] Due to its higher vapor pressure, the water confined inside the nanotubes' cavity can evaporate faster than the bulk water. The difference of the water evaporation rate represents the main driving force for the filling of HNTs cavity through aqueous dispersions. Interestingly, we observed that the surfactant hydrophobization of the halloysite lumen does not alter the water confinement. On this basis, we can assert that the chemical composition of the HNTs inner surface does not influence the confinement process. Contrary to halloysite nanotubes, the water evaporated from kaolinite dispersion possesses $(dm/dt)_n/(dm/dt)_w \leq 1$ within the entire evaporation process (Figure 2) evidencing that the platy morphology did not provide any confinement site for the aqueous solvent. As sketched in Figure 3, we can conclude that the water confinement is totally related to the geometrical characteristics of the nanoclay particles.

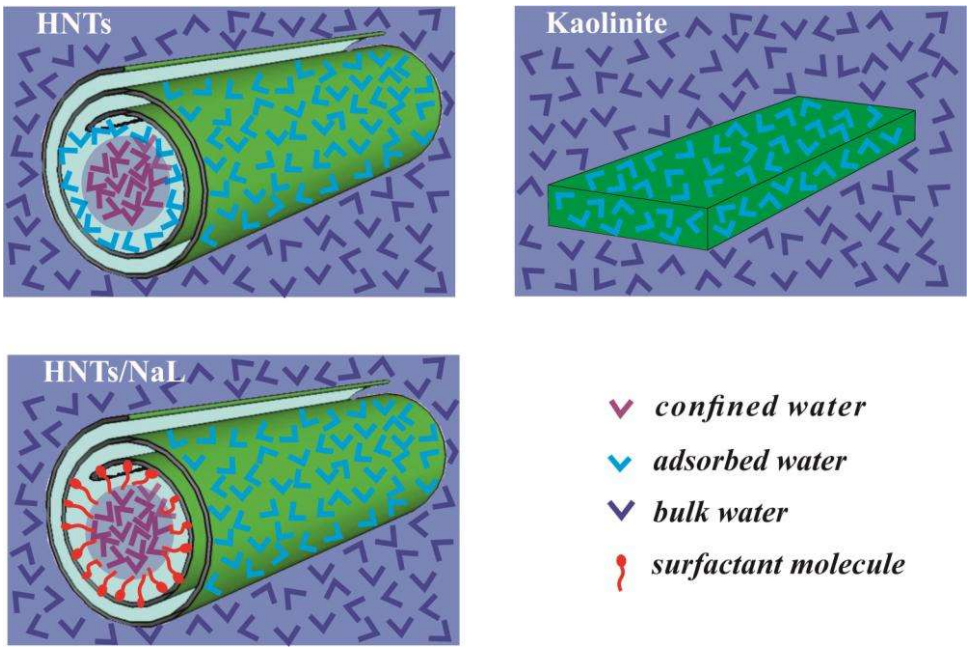

Figure 3. Schematic representation of the water confinement process within clay nanoparticles. The comparison between halloysite nanotubes and platy kaolinite.

3.1.2 Water adsorption onto nanoclay surfaces

Water molecules with $(dm/dt)_n/(dm/dt)_w < 1$ are related to the isothermal desorption from the nanoclays surfaces occurring during the evaporation process. As shown in Figure 2, the desorption isotherms were successfully fitted by using the Guggenheim-Anderson-de Boer (GAB) model,[53] which is expressed by the following equation

$$M_w = (M_0 \cdot C \cdot K \cdot a_w)/[(1-K \cdot a_w) \cdot (1-K \cdot a_w + C \cdot K \cdot a_w)] \quad (4)$$

where M_0 is the monolayer moisture content, while C and K are adsorption constants associated to the monolayer and the upper multilayers, respectively.

It should be noted that the GAB equation is valid for $0.05 \leq a_w \leq 0.95$. The suitability of GAB model for the experimental desorption isotherms was proved by the K values, which range between 0 and 1 as requested for the validation of this approach.

Table 1 collects the adsorption parameters calculated for HNTs, HNTs/NaL and kaolinite.

Table 1. GAB fitting parameters for the water desorption from nanoclays.

Nanoclay	M_0	K	C
HNTs	$(2.72 \pm 0.11) \cdot 10^{-2}$	0.78 ± 0.01	7.1 ± 0.7
HNTs/NaL	$(1.46 \pm 0.03) \cdot 10^{-2}$	0.885 ± 0.007	15.1 ± 1.2
Kaolinite	$(0.37 \pm 0.09) \cdot 10^{-2}$	0.979 ± 0.001	7 ± 2

Regarding the monolayer moisture content, we detected that M_0 of kaolinite is much lower compared to those of both pure and modified HNTs. Based on M_0 values, the specific surface area (SSA) for water sorption can be determined as[54]

$$SSA = (M_0 \cdot N_A \cdot A_w) / MM_w \quad (5)$$

being N_A the Avogadro number, whereas A_w and MM_w are the surface area and the molecular weight of water, respectively. According to the morphological characteristics, kaolinite possesses a smaller SSA respect to that of halloysite. Namely, the rolling of kaolinite plates into halloysite nanotubes generates an enhancement of the surface area because of geometrical considerations.

Table 2. Specific surface area of the nanoclays determined by the fitting of water desorption isotherms.

Nanoclay	SSA / m^2 g^{-1}
HNTs	96 ± 4
HNTs/NaL	51.9 ± 1.3
Kaolinite	13.4 ± 0.3

The surfactant modification of halloysite inner surface determined a SSA decrease that cannot be ascribed to morphological variations. As displayed by FESEM micrographs (Figure 1), HNTs/NaL preserves the hollow tubular morphology of HNTs and the sizes of pure and modified halloysite are comparable. On the other hand, the SSA reduction can be attributed to changes on the chemical composition of halloysite inner surface. Specifically, pristine HNTs possess a hydrophilic lumen that allows for the water adsorption onto the internal surface. In contrast, water molecules cannot be adsorbed within the hydrophobically modified cavity of HNTs/NaL. HNTs exhibits two hydrophilic adsorption sites (outer and inner surfaces), while the water sorption is limited to the HNTs/NaL outer shell. As concerns the adsorption constants, we calculated C values larger than K for all the nanoclays highlighting that the adsorption heat of the first water layer is higher respect to that of the multilayers.[55] This difference was enhanced by the hydrophobization of the HNTs cavity. As general result, the desorption isotherms can be classified as type III being that C is larger than 2.[53]

3.2 Wettability of nanoclays

The wettability properties of HNTs, HNTs/NaL and kaolinite were investigated by water contact angle experiments. Figure 4a shows the images of the water droplets just after their deposition on the nanoclay surface. According to their chemical composition, kaolinite and HNTs exhibited a hydrophilic surface as demonstrated by their θ_i values (30.1 and 30.7°, respectively). Interestingly, the hydrophobization of the HNTs cavity did not alter the hydrophilic behavior of the halloysite surface in agreement with the selective adsorption of the anionic NaL inside the lumen. Similar results were detected for HNTs modified with negatively charged polymers, such as polystyrene sulfonate.[27]

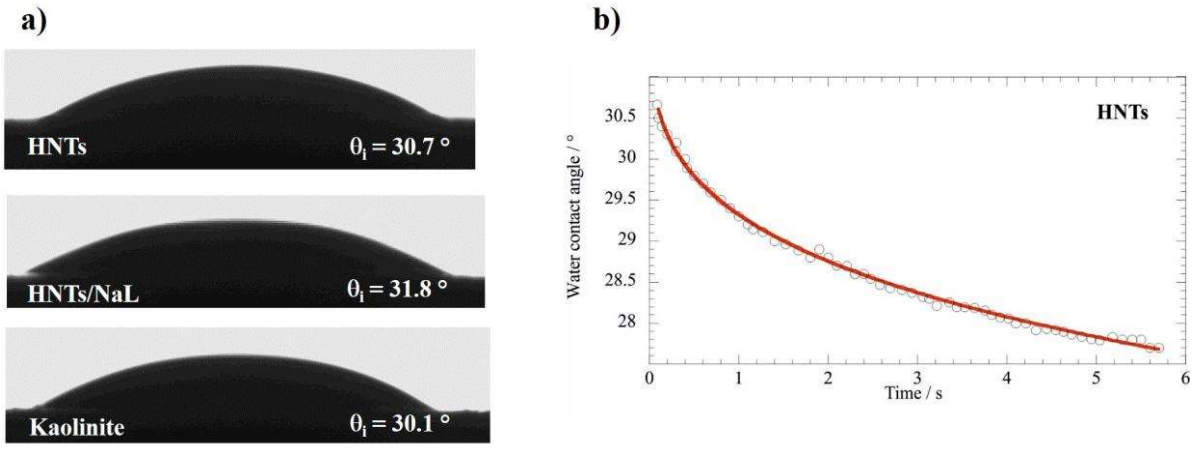

Figure 4. a) Images of the water droplets just after their deposition on the surface of HNTs, HNTs/NaL and kaolinite. The corresponding θ_i are reported. b) The water contact angle as a function of time for HNTs. The solid red line represents the fitting based on the equation 3.

Additional information on the interactions between water and nanoclay surface were obtained by the analysis of the kinetic evolution of the water contact angle. As displayed in Figure 4b for HNTs, the θ vs t trends were successfully fitted by the equation 1 providing the kinetic constant and the n exponential parameter, which are collected in Table 3.

Table 3. Fitting parameters on the kinetic evolution of the water contact angle

Nanoclay	k_θ / s^{-1}	n
HNTs	0.087 ± 0.009	0.28 ± 0.02
HNTs/NaL	0.036 ± 0.003	0.65 ± 0.02
Kaolinite	0.063 ± 0.011	0.82 ± 0.06

The goodness of the equation 1 as model fitting for the θ vs t functions was proved by the n values, which range between 0 and 1 indicating that the kinetic evolution of the contact angle is affected by both the absorption and the spreading of water onto the nanoclay surface. The presence of NaL within the HNTs lumen generated a decrease of the process rate and an enhancement of the spreading contribution, which is evidenced by the n reduction.

The combination of the water contact angle with Knudsen thermogravimetry data allowed us to estimate the cavity radius (r_c) of HNTs and HNTs/NaL. According to the La Place-Kelvin equation, r_c can be calculated by θ_i and the ratio between the vapor pressure of confined water (P) and bulk water (P°) as

$$r_c = (2 \cdot \gamma_w \cdot V_w \cdot \cos(\theta_i))/(R \cdot T \cdot \ln(P/P°)) \quad (5)$$

where γ_w and V_w are the surface tension and the molar volume of water, T is the temperature and R is the ideal gas constant.

Based on the KTG analysis (Figure 1), the confinement process within the halloysite lumen was proved by the detection of evaporating water molecules with $(dm/dt)_n/(dm/dt)_w > 1$. Assuming that P/P° corresponds to the largest $(dm/dt)_n/(dm/dt)_w$ value, r_c = 9.0 ± 0.2 and 11.7 ± 0.2 nm were calculated for HNTs and HNTs/NaL, respectively. These results are consistent with the structural investigations of halloysite nanotubes reported in literature.[21,22]

3.3 The effect of the vacuum pumping on the guest molecules loading within HNTs cavity

We investigated the effect of the pressure conditions on the loading efficiency of HNTs towards several bioactive compounds including metoprolol tartrate (MT), salicylic acid (SA) and malonic acid (MA). In particular, the filling of HNTs lumen was conducted by aqueous solutions of the guest molecules exposed at ambient pressure (P = 1 atm) as well as under forced reduced pressure (P = 0.01 atm). The amount of active molecules loaded into the HNTs cavity was determined through thermogravimetry. Figure 5a compares the thermogravimetric curves of pristine halloysite and HNTs filled with malonic acid.

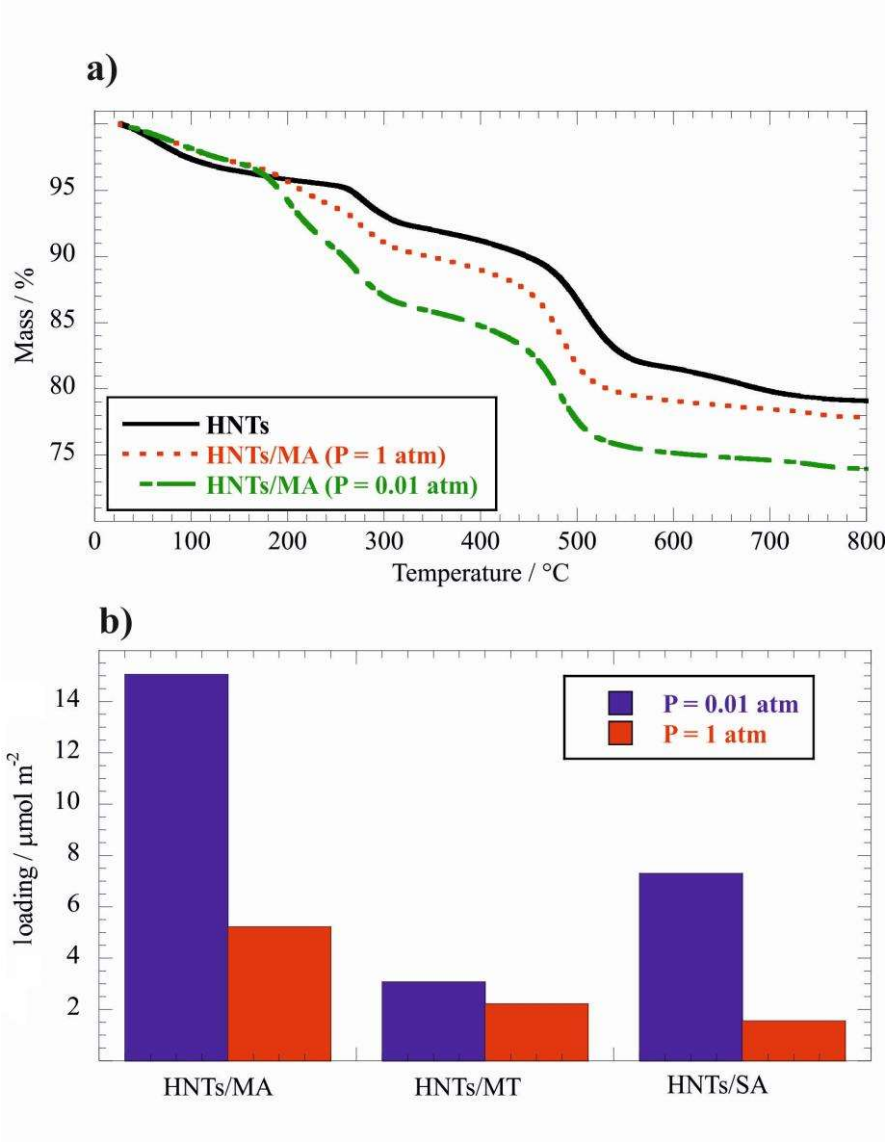

Figure 5. a) Thermogravimetric curves for HNTs and HNTs loaded with malonic. b) Loadings for HNTs filled with malonic acid, metoprolol tartrate and salicylic acid.

As expected, the presence of the active molecules generated a decrease of the residual mass at high temperature because the organic moiety thermally decomposes in the range from 200 to 400 °C (see Supporting Information). The nanotubes loaded under vacuum exhibited a lower residual matter with respect to that prepared at ambient pressure highlighting the better loading efficiency at reduced pressure. As reported elsewhere,[33] we calculated the amount of active molecules encapsulated inside HNTs by using the rule of mixtures on the residual masses at 800 °C. Figure 5b presents the loading results as surface molar coverage (μmol of guest molecule per m^2 of halloysite surface), while Table 4 collects the mass percentages of the guest molecules in HNTs based hybrids. It should be noted that the active molecules possess anionic carboxylate groups in their chemical structure. Accordingly, the loading process is favored by the attractive interactions between the guest molecules and the halloysite inner surface, which is positively charged.

Table 4. Mass percentages of the guest molecules filled into halloysite nanotubes

Hybrid nanomaterial	Loading / wt%	
	P = 1 atm	P = 0.01 atm
HNTs/MA	2.52 ± 0.12	7.3 ± 0.3
HNTs/MT	2.77 ± 0.13	3.84 ± 0.19
HNTs/SA	1.01 ± 0.07	4.7 ± 0.2

As a general result, an enhancement of the loading efficiency was determined by the reduction of the pressure confirming that the vacuum favors the filling of the HNTs cavity. In detail, the amount of guest molecule incorporated within the nanotubes increased by 38, 188 and 369 % for MT, MA and SA, respectively. Contrary to these results, the loading capacity of kaolinite was slightly affected by the pressure conditions in agreement with its platy morphology. As shown in Supporting Information, we detected similar thermogravimetric curves for kaolinite/SA samples prepared at different pressure. In particular, the residual matter at 800 °C was not significantly

altered by vacuum application and, consequently, similar SA loadings (0.45 and 0.62 wt% for the hybrids prepared at P = 1 and 0.01 atm, respectively) were estimated through the rule of mixtures. Morphological investigations of loaded HNTs confirmed that a lower pressure increases the filling of the halloysite lumen. In this regards, Figure 6 shows FESEM images of HNTs/MA samples prepared at different pressure conditions.

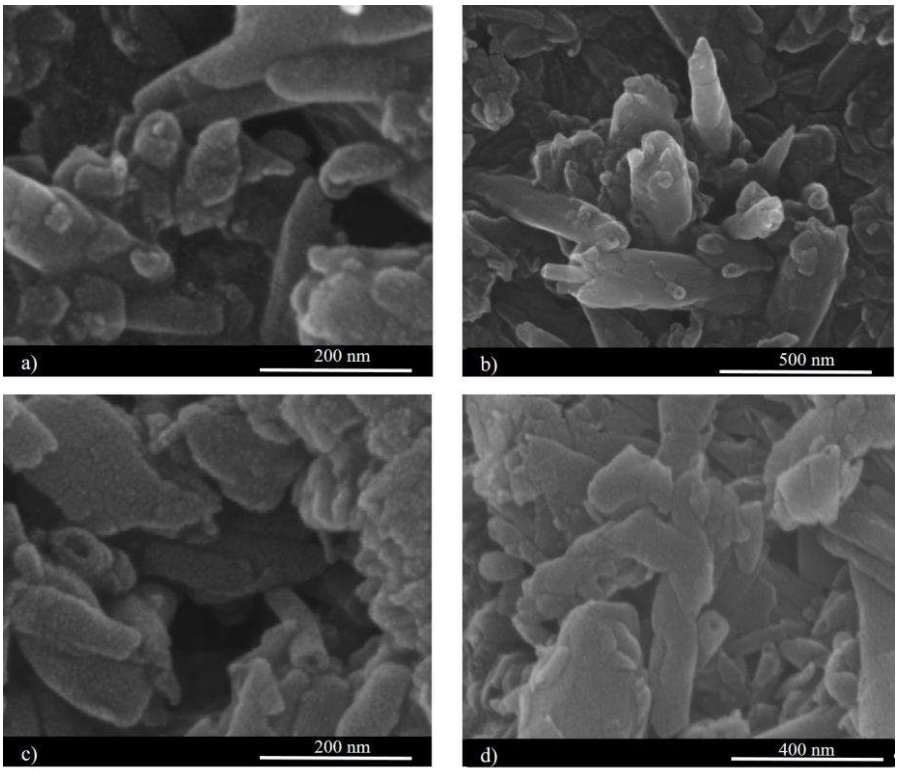

Figure 6. FESEM images for HNTs/MA prepared at P = 0.01 atm (a,b) and 1 atm (c,d)

As a general result, the loading did not significantly modify the halloysite tubular morphology. Halloysite loaded at P = 0.01 atm (Figures 6a,b) evidenced several nanotubes fully closed with some spherical nanoparticles at the lumen gate as a consequence of the MA filling. This peculiarity was not observed for HNTs/MA prepared at P = 1 atm (Figure 6c,d). Namely, halloysite filled at ambient pressure preserved the hollow cavity indicating a lower loading efficiency.

The influence of the pressure conditions on the loading of halloysite is strictly correlated to the water confinement within HNTs cavity proved by Knudsen thermogravimetry. As sketched in Figure 7, the filling of the HNTs cavity is due to the different volatility of confined and bulk water.

The fraction of water confined into the lumen possess a larger vapor pressure compared to that of the bulk water generating a difference in the evaporation rate. Based on KTG measurements at 30 °C, confined water presents a vapor pressure equals to 0.0460 ± 0.0008 atm, which is 12% larger than that of bulk water (0.0419 atm) and, consequently, a flux of water from the bulk phase to the confined part is needed to compensate the different evaporation velocity and to refill the lumen. Namely, the faster evaporation of the confined water determines a flux of the aqueous solution within the HNTs cavity and a consequent enrichment of the entrapped guest molecules. Then, the evaporation of aqueous solvent causes the precipitation of the active molecules within the HNTs lumen. The replacement of the aqueous solution inside the halloysite lumen is facilitated under low-pressure conditions because the water vapor pressure is approaching. Consequently, the solvent volatilization rate increases.

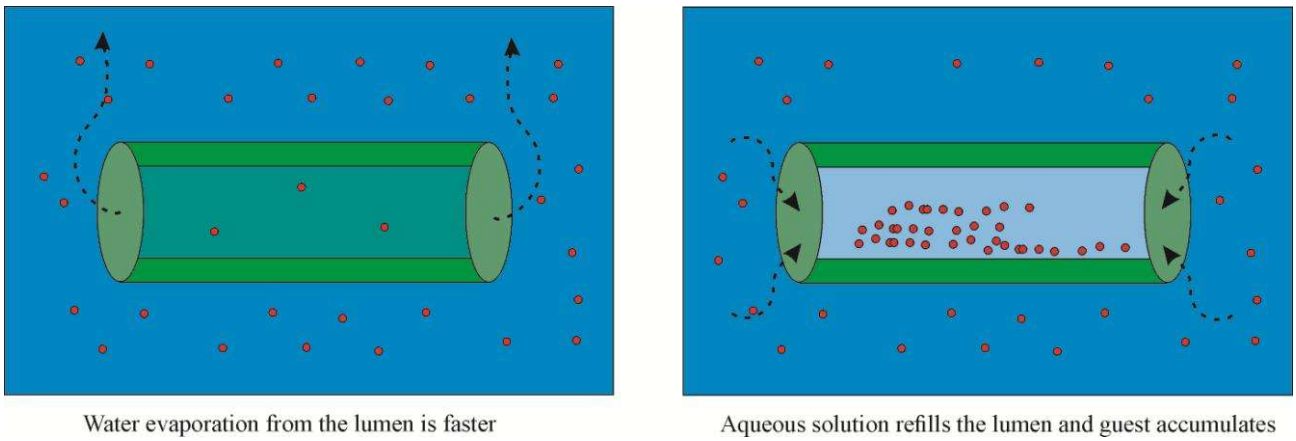

Figure 7. Schematic representation on the filling process of halloysite nanotubes.

4. Conclusions

This work represents the first thermodynamic demonstration of the water confinement within the cavity of halloysite nanotubes (HNTs). The water confinement was not observed in kaolinite nanosheets, while this process occurred in HNTs/sodium dodecanoate hybrid highlighting that water molecules can be confined within halloysite nanotubes with a hydrophobically modified cavity. The thermodynamic evidence of the water confinement is the starting point for a proper

description of the loading mechanism of HNTs cavity from aqueous solutions of guest molecules. Compared to the bulk water, the confined fraction exhibits a larger vapor pressure and, consequently, a faster evaporation rate that can be attributed to the Gibbs-Thomson effect. During the water evaporation, the guest molecules precipitate inside the cavity and fresh aqueous solution from bulk phase migrates to the halloysite lumen. This phenomenon is favored by vacuum pumping once that vapor pressure of the solvent is approached. The latter was experimentally proved by loading three different guest molecules with anionic carboxylate groups, which can interact with the positive HNT internal surface because of electrostatic attractions. In this regards, we observed that the vacuum pumping operation induces relevant increases on the loading efficiency of halloysite nanotubes. The amount of salicylic acid filled into the HNTs lumen was enhanced by 369% as a consequence of the cyclic vacuum pumping in/out procedure. In contrast, the loading capacity of kaolinite nanosheets was not significantly altered by vacuum application.

In conclusion, this study describes the physico-chemical aspects of halloysite filling, which is controlled by water confinement within the nanotubes' cavity. The attained knowledge represents a fundamental step for the development of loading protocols into confined spaces of tubular nanoparticles.

Supporting Information

Knudsen thermogravimetric curves for HNTs, HNTs/NaL and kaolinite aqueous dispersions. Thermogravimetric curve for malonic acid. Thermogravimetric curves for kaolinite and kaolinite/salicylic acid hybrids prepared at different pressure conditions.

Acknowledgments

The work was financially supported by Progetto di ricerca e sviluppo "AGM for CuHe" (ARS01_00697) and University of Palermo.

References

(1) Kim, B. M.; Qian, S.; Bau, H. H. Filling Carbon Nanotubes with Particles. *Nano Lett.* **2005**, *5* (5), 873–878. https://doi.org/10.1021/nl050278v.

(2) Chaban, V. V.; Prezhdo, O. V. Water Boiling Inside Carbon Nanotubes: Toward Efficient Drug Release. *ACS Nano* **2011**, *5* (7), 5647–5655. https://doi.org/10.1021/nn201277a.

(3) Lazzara, G.; Cavallaro, G.; Panchal, A.; Fakhrullin, R.; Stavitskaya, A.; Vinokurov, V.; Lvov, Y. An Assembly of Organic-Inorganic Composites Using Halloysite Clay Nanotubes. *Curr. Opin. Colloid Interface Sci.* **2018**, *35*, 42–50. https://doi.org/10.1016/j.cocis.2018.01.002.

(4) Wu, S.; Qiu, M.; Guo, B.; Zhang, L.; Lvov, Y. Nanodot-Loaded Clay Nanotubes as Green and Sustained Radical Scavengers for Elastomer. *ACS Sustainable Chem. Eng.* **2017**, *5* (2), 1775–1783. https://doi.org/10.1021/acssuschemeng.6b02523.

(5) Joo, Y.; Sim, J. H.; Jeon, Y.; Lee, S. U.; Sohn, D. Opening and Blocking the Inner-Pores of Halloysite. *Chem. Commun.* **2013**, *49* (40), 4519–4521. https://doi.org/10.1039/C3CC40465J.

(6) Zhuang, Z.; Chen, W. Ultra-Low Loading of Pd5 Nanoclusters on Carbon Nanotubes as Bifunctional Electrocatalysts for the Oxygen Reduction Reaction and the Ethanol Oxidation Reaction. *J Colloid Interface Sci.* **2019**, *538*, 699–708. https://doi.org/10.1016/j.jcis.2018.12.015.

(7) Yu, Y.-D.; Zhu, Y.-J.; Qi, C.; Jiang, Y.-Y.; Li, H.; Wu, J. Hydroxyapatite Nanorod-Assembled Porous Hollow Polyhedra as Drug/Protein Carriers. *J Colloid Interface Sci.* **2017**, *496*, 416–424. https://doi.org/10.1016/j.jcis.2017.02.041.

(8) Jiang, L.; Huang, Y.; Liu, T. Enhanced Visible-Light Photocatalytic Performance of Electrospun Carbon-Doped TiO2/Halloysite Nanotube Hybrid Nanofibers. *J Colloid Interface Sci.* **2015**, *439*, 62–68. https://doi.org/10.1016/j.jcis.2014.10.026.

(9) Liu, F.; Bai, L.; Zhang, H.; Song, H.; Hu, L.; Wu, Y.; Ba, X. Smart H2O2-Responsive Drug Delivery System Made by Halloysite Nanotubes and Carbohydrate Polymers. *ACS Appl. Mater. Interfaces* **2017**, *9* (37), 31626–31633. https://doi.org/10.1021/acsami.7b10867.

(10) Sadjadi, S.; Heravi, M. M.; Malmir, M. Pd@HNTs-CDNS-g-C3N4: A Novel Heterogeneous Catalyst for Promoting Ligand and Copper-Free Sonogashira and Heck Coupling Reactions, Benefits from Halloysite and Cyclodextrin Chemistry and g-C3N4 Contribution to Suppress Pd Leaching. *Carbohydr. Polym.* **2018**, *186*, 25–34. https://doi.org/10.1016/j.carbpol.2018.01.023.

(11) Sadjadi, S.; Heravi, M. M.; Kazemi, S. S. Ionic Liquid Decorated Chitosan Hybridized with Clay: A Novel Support for Immobilizing Pd Nanoparticles. *Carbohydr. Polym.* **2018**, *200*, 183–190. https://doi.org/10.1016/j.carbpol.2018.07.093.

(12) Liu, Y.; Zhang, J.; Guan, H.; Zhao, Y.; Yang, J.-H.; Zhang, B. Preparation of Bimetallic Cu-Co Nanocatalysts on Poly (Diallyldimethylammonium Chloride) Functionalized Halloysite Nanotubes for Hydrolytic Dehydrogenation of Ammonia Borane. *Appl Surf Sci* **2018**, *427*, 106–113. https://doi.org/10.1016/j.apsusc.2017.08.171.

(13) Liu, Y.; Guan, H.; Zhang, J.; Zhao, Y.; Yang, J.-H.; Zhang, B. Polydopamine-Coated Halloysite Nanotubes Supported AgPd Nanoalloy: An Efficient Catalyst for Hydrolysis of Ammonia Borane. *Int. J. Hydrogen Energ.* **2018**, *43* (5), 2754–2762. https://doi.org/10.1016/j.ijhydene.2017.12.105.

(14) Fakhrullina, G. I.; Akhatova, F. S.; Lvov, Y. M.; Fakhrullin, R. F. Toxicity of Halloysite Clay Nanotubes in Vivo: A Caenorhabditis Elegans Study. *Environ. Sci.: Nano* **2015**, *2* (1), 54–59. https://doi.org/10.1039/C4EN00135D.

(15) Wang, X.; Gong, J.; Rong, R.; Gui, Z.; Hu, T.; Xu, X. Halloysite Nanotubes-Induced Al Accumulation and Fibrotic Response in Lung of Mice after 30-Day Repeated Oral

Administration. *J. Agric. Food Chem.* **2018**, *66* (11), 2925–2933. https://doi.org/10.1021/acs.jafc.7b04615.
(16) Cavallaro, G.; Lazzara, G.; Milioto, S.; Parisi, F.; Evtugyn, V.; Rozhina, E.; Fakhrullin, R. Nanohydrogel Formation within the Halloysite Lumen for Triggered and Sustained Release. *ACS Appl. Mater. Inter.* **2018**, *10* (9), 8265–8273. https://doi.org/10.1021/acsami.7b19361.
(17) Makaremi, M.; Pasbakhsh, P.; Cavallaro, G.; Lazzara, G.; Aw, Y. K.; Lee, S. M.; Milioto, S. Effect of Morphology and Size of Halloysite Nanotubes on Functional Pectin Bionanocomposites for Food Packaging Applications. *ACS Appl. Mater. Inter* **2017**, *9* (20), 17476–17488. https://doi.org/10.1021/acsami.7b04297.
(18) Tarasova, E.; Naumenko, E.; Rozhina, E.; Akhatova, F.; Fakhrullin, R. Cytocompatibility and Uptake of Polycations-Modified Halloysite Clay Nanotubes. *App Clay Sci* **2019**, *169*, 21–30. https://doi.org/10.1016/j.clay.2018.12.016.
(19) Ahmed, F. R.; Shoaib, M. H.; Azhar, M.; Um, S. H.; Yousuf, R. I.; Hashmi, S.; Dar, A. In-Vitro Assessment of Cytotoxicity of Halloysite Nanotubes against HepG2, HCT116 and Human Peripheral Blood Lymphocytes. *Colloids Surf. B Biointerfaces* **2015**, *135*, 50–55. https://doi.org/10.1016/j.colsurfb.2015.07.021.
(20) Vergaro, V.; Abdullayev, E.; Lvov, Y. M.; Zeitoun, A.; Cingolani, R.; Rinaldi, R.; Leporatti, S. Cytocompatibility and Uptake of Halloysite Clay Nanotubes. *Biomacromolecules* **2010**, *11* (3), 820–826. https://doi.org/10.1021/bm9014446.
(21) Pasbakhsh, P.; Churchman, G. J.; Keeling, J. L. Characterisation of Properties of Various Halloysites Relevant to Their Use as Nanotubes and Microfibre Fillers. *Appl. Clay Sci.* **2013**, *74*, 47–57. https://doi.org/10.1016/j.clay.2012.06.014.
(22) Cavallaro, G.; Chiappisi, L.; Pasbakhsh, P.; Gradzielski, M.; Lazzara, G. A Structural Comparison of Halloysite Nanotubes of Different Origin by Small-Angle Neutron Scattering (SANS) and Electric Birefringence. *App Clay Sci* **2018**, *160*, 71–80. https://doi.org/10.1016/j.clay.2017.12.044.
(23) Joussein, E.; Petit, S.; Churchman, G. J.; Theng, B.; Righi, D.; Delvaux, B. Halloysite Clay Minerals — a Review. *Clay Miner* **2005**, *40* (4), 383–426.
(24) Zhang, H.; Ren, T.; Ji, Y.; Han, L.; Wu, Y.; Song, H.; Bai, L.; Ba, X. Selective Modification of Halloysite Nanotubes with 1-Pyrenylboronic Acid: A Novel Fluorescence Probe with Highly Selective and Sensitive Response to Hyperoxide. *ACS Appl. Mater. Interfaces* **2015**, *7* (42), 23805–23811. https://doi.org/10.1021/acsami.5b08600.
(25) Cavallaro, G.; Grillo, I.; Gradzielski, M.; Lazzara, G. Structure of Hybrid Materials Based on Halloysite Nanotubes Filled with Anionic Surfactants. *J. Phys. Chem. C* **2016**, *120* (25), 13492–13502. https://doi.org/10.1021/acs.jpcc.6b01282.
(26) Cavallaro, G.; Lazzara, G.; Milioto, S.; Parisi, F.; Sanzillo, V. Modified Halloysite Nanotubes: Nanoarchitectures for Enhancing the Capture of Oils from Vapor and Liquid Phases. *ACS Appl. Mater. Interfaces* **2014**, *6* (1), 606–612. https://doi.org/10.1021/am404693r.
(27) Zhao, Y.; Cavallaro, G.; Lvov, Y. Orientation of Charged Clay Nanotubes in Evaporating Droplet Meniscus. *J Colloid Interface Sci.* **2015**, *440* (0), 68–77. https://doi.org/10.1016/j.jcis.2014.10.050.
(28) Liu, M.; Huo, Z.; Liu, T.; Shen, Y.; He, R.; Zhou, C. Self-Assembling Halloysite Nanotubes into Concentric Ring Patterns in a Sphere-on-Flat Geometry. *Langmuir* **2017**, *33* (12), 3088–3098. https://doi.org/10.1021/acs.langmuir.6b04460.
(29) Luo, Z.; Song, H.; Feng, X.; Run, M.; Cui, H.; Wu, L.; Gao, J.; Wang, Z. Liquid Crystalline Phase Behavior and Sol–Gel Transition in Aqueous Halloysite Nanotube Dispersions. *Langmuir* **2013**, *29* (40), 12358–12366. https://doi.org/10.1021/la402836d.
(30) Owoseni, O.; Nyankson, E.; Zhang, Y.; Adams, S. J.; He, J.; McPherson, G. L.; Bose, A.; Gupta, R. B.; John, V. T. Release of Surfactant Cargo from Interfacially-Active Halloysite Clay Nanotubes for Oil Spill Remediation. *Langmuir* **2014**, *30* (45), 13533–13541. https://doi.org/10.1021/la503687b.

(31) von Klitzing, R.; Stehl, D.; Pogrzeba, T.; Schomäcker, R.; Minullina, R.; Panchal, A.; Konnova, S.; Fakhrullin, R.; Koetz, J.; Möhwald, H.; et al. Halloysites Stabilized Emulsions for Hydroformylation of Long Chain Olefins. *Adv. Mater. Interf.* **2016**, 1600435-n/a. https://doi.org/10.1002/admi.201600435.
(32) Cavallaro, G.; Milioto, S.; Parisi, F.; Lazzara, G. Halloysite Nanotubes Loaded with Calcium Hydroxide: Alkaline Fillers for the Deacidification of Waterlogged Archeological Woods. *ACS Appl. Mater. Inter* **2018**, *10* (32), 27355–27364. https://doi.org/10.1021/acsami.8b09416.
(33) Massaro, M.; Cavallaro, G.; Colletti, C. G.; D'Azzo, G.; Guernelli, S.; Lazzara, G.; Pieraccini, S.; Riela, S. Halloysite Nanotubes for Efficient Loading, Stabilization and Controlled Release of Insulin. *J Colloid Interface Sci.* **2018**, *524*, 156–164. https://doi.org/10.1016/j.jcis.2018.04.025.
(34) Abdullayev, E.; Lvov, Y. Halloysite Clay Nanotubes as a Ceramic "Skeleton" for Functional Biopolymer Composites with Sustained Drug Release. *J. Mater. Chem. B* **2013**, *1* (23), 2894–2903. https://doi.org/10.1039/C3TB20059K.
(35) Lvov, Y.; Wang, W.; Zhang, L.; Fakhrullin, R. Halloysite Clay Nanotubes for Loading and Sustained Release of Functional Compounds. *Adv Mater* **2016**, *28* (6), 1227–1250. https://doi.org/10.1002/adma.201502341.
(36) Kurczewska, J.; Cegłowski, M.; Messyasz, B.; Schroeder, G. Dendrimer-Functionalized Halloysite Nanotubes for Effective Drug Delivery. *App Clay Sci* **2018**, *153*, 134–143. https://doi.org/10.1016/j.clay.2017.12.019.
(37) Abdullayev, E.; Sakakibara, K.; Okamoto, K.; Wei, W.; Ariga, K.; Lvov, Y. Natural Tubule Clay Template Synthesis of Silver Nanorods for Antibacterial Composite Coating. *ACS Appl. Mater. Interfaces* **2011**, *3* (10), 4040–4046. https://doi.org/10.1021/am200896d.
(38) Ouyang, J.; Guo, B.; Fu, L.; Yang, H.; Hu, Y.; Tang, A.; Long, H.; Jin, Y.; Chen, J.; Jiang, J. Radical Guided Selective Loading of Silver Nanoparticles at Interior Lumen and out Surface of Halloysite Nanotubes. *Mater Design* **2016**, *110*, 169–178. https://doi.org/10.1016/j.matdes.2016.07.127.
(39) Zhong, B.; Lin, J.; Liu, M.; Jia, Z.; Luo, Y.; Jia, D.; Liu, F. Preparation of Halloysite Nanotubes Loaded Antioxidant and Its Antioxidative Behaviour in Natural Rubber. *Polym. Degrad. Stab.* **2017**, *141*, 19–25. https://doi.org/10.1016/j.polymdegradstab.2017.05.009.
(40) Du, M.; Guo, B.; Jia, D. Newly Emerging Applications of Halloysite Nanotubes: A Review. *Polym. Int.* **2010**, *59* (5), 574–582.
(41) Abdullayev, E.; Price, R.; Shchukin, D.; Lvov, Y. Halloysite Tubes as Nanocontainers for Anticorrosion Coating with Benzotriazole. *ACS Appl. Mater. Interfaces* **2009**, *1* (7), 1437–1443. https://doi.org/10.1021/am9002028.
(42) Gorrasi, G. Dispersion of Halloysite Loaded with Natural Antimicrobials into Pectins: Characterization and Controlled Release Analysis. *Carbohydr. Polym.* **2015**, *127*, 47–53. https://doi.org/10.1016/j.carbpol.2015.03.050.
(43) Pierchala, M. K.; Makaremi, M.; Tan, H. L.; Pushpamalar, J.; Muniyandy, S.; Solouk, A.; Lee, S. M.; Pasbakhsh, P. Nanotubes in Nanofibers: Antibacterial Multilayered Polylactic Acid/Halloysite/Gentamicin Membranes for Bone Regeneration Application. *App Clay Sci* **2018**, *160*, 95–105. https://doi.org/https://doi.org/10.1016/j.clay.2017.12.016.
(44) Price. In Vitro Release Characteristics of Tetracyline HCl, Khellin and Nicotinamide Adenine Dinucloetide from Halloysite; a Cylindrical Mineral. *J. Microencapsul.* **2001**, *18* (6), 713.
(45) Shchukin, D. G.; Lamaka, S. V.; Yasakau, K. A.; Zheludkevich, M. L.; Ferreira, M. G. S.; Mohwald, H. Active Anticorrosion Coatings with Halloysite Nanocontainers. *J. Phys. Chem. C* **2008**, *112* (4), 958–964. https://doi.org/doi: 10.1021/jp076188r.
(46) Lvov, Y. M.; Shchukin, D. G.; Mohwald, H.; Price, R. R. Halloysite Clay Nanotubes for Controlled Release of Protective Agents. *ACS Nano* **2008**, *2* (5), 814–820. https://doi.org/doi: 10.1021/nn800259q.

(47) Rao, K. M.; Nagappan, S.; Seo, D. J.; Ha, C.-S. PH Sensitive Halloysite-Sodium Hyaluronate/Poly(Hydroxyethyl Methacrylate) Nanocomposites for Colon Cancer Drug Delivery. *App Clay Sci* **2014**, *97–98*, 33–42. https://doi.org/10.1016/j.clay.2014.06.002.
(48) Cavallaro, G.; Lazzara, G.; Milioto, S. Exploiting the Colloidal Stability and Solubilization Ability of Clay Nanotubes/Ionic Surfactant Hybrid Nanomaterials. *J. Phys. Chem. C* **2012**, *116* (41), 21932–21938. https://doi.org/10.1021/jp307961q.
(49) Blanco, I.; Abate, L.; Bottino, F. A.; Bottino, P. Thermal Behaviour of a Series of Novel Aliphatic Bridged Polyhedral Oligomeric Silsesquioxanes (POSSs)/Polystyrene (PS) Nanocomposites: The Influence of the Bridge Length on the Resistance to Thermal Degradation. *Polym. Degrad. Stab.* **2014**, *102* (0), 132–137. https://doi.org/10.1016/j.polymdegradstab.2014.01.029.
(50) Clausen, P.; Signorelli, M.; Schreiber, A.; Hughes, E.; Plummer, C. J. G.; Fessas, D.; Schiraldi, A.; Månson, J.-A. E. Equilibrium Desorption Isotherms of Water, Ethanol, Ethyl Acetate, and Toluene on a Sodium Smectite Clay. *J Therm Anal Calorim* **2009**, *98* (3), 833–841. https://doi.org/10.1007/s10973-009-0003-x.
(51) Farris, S.; Introzzi, L.; Biagioni, P.; Holz, T.; Schiraldi, A.; Piergiovanni, L. Wetting of Biopolymer Coatings: Contact Angle Kinetics and Image Analysis Investigation. *Langmuir* **2011**, *27* (12), 7563–7574. https://doi.org/doi: 10.1021/la2017006.
(52) Johnston, J. C.; Molinero, V. Crystallization, Melting, and Structure of Water Nanoparticles at Atmospherically Relevant Temperatures. *J. Am. Chem. Soc.* **2012**, *134* (15), 6650–6659. https://doi.org/10.1021/ja210878c.
(53) Fotie, G.; Rampazzo, R.; Ortenzi, A. M.; Checchia, S.; Fessas, D.; Piergiovanni, L. The Effect of Moisture on Cellulose Nanocrystals Intended as a High Gas Barrier Coating on Flexible Packaging Materials. *Polymers* **2017**, *9* (9). https://doi.org/10.3390/polym9090415.
(54) Arslan, N.; Togˇrul, H. The Fitting of Various Models to Water Sorption Isotherms of Tea Stored in a Chamber under Controlled Temperature and Humidity. *J Stored Prod Res* **2006**, *42* (2), 112–135. https://doi.org/10.1016/j.jspr.2005.01.001.
(55) Yogendrarajah, P.; Samapundo, S.; Devlieghere, F.; De Saeger, S.; De Meulenaer, B. Moisture Sorption Isotherms and Thermodynamic Properties of Whole Black Peppercorns (Piper Nigrum L.). *Food Sci. Technol. Int.* **2015**, *64* (1), 177–188. https://doi.org/10.1016/j.lwt.2015.05.045.